IEEE Access
Multidisciplinary | Rapid Review | Open Access Journal

Received July 25, 2019, accepted August 31, 2019, date of publication September 5, 2019, date of current version September 18, 2019.

Digital Object Identifier 10.1109/ACCESS.2019.2939648

Liquid Crystal Based Dielectric Waveguide Phase Shifters for Phased Arrays at W-Band

ROLAND REESE, (Student Member, IEEE), ERSIN POLAT, (Student Member, IEEE), HENNING TESMER, (Student Member, IEEE), JONATHAN STROBL, CHRISTIAN SCHUSTER, (Student Member, IEEE), MATTHIAS NICKEL, (Student Member, IEEE), ANGEL BLANCO GRANJA, (Student Member, IEEE), ROLF JAKOBY, (Member, IEEE), AND HOLGER MAUNE, (Senior Member, IEEE)
Institute for Microwave Engineering and Photonics, Technische Universität Darmstadt, 64283 Darmstadt, Germany

Corresponding author: Roland Reese (reese@imp.tu-darmstadt.de)

This work was supported in part by the Marie Curie European Training Networks ITN CELTA from the European Union's Horizon2020 Research and Innovation Programme under Contract 675683. We acknowledge support by the German Research Foundation and the Open Access Publishing Fund of Technische Universität Darmstadt.

ABSTRACT In this work, the feasibility of microwave liquid crystal based dielectric waveguide phased shifters is investigated in a phased rod antenna array for the first time. For this, a 1×4 rod antenna array is designed including the phase shifters as well as a cascaded E-plane power divider network. As core elements, the phase shifter are designed as continuously tunable subwavelength fibers, partially filled with a newly specifically synthesized microwave liquid crystal, exhibiting a maximum FoM 145°/dB at 102.5 GHz. As proof-of-concept, a simplified electric biasing network is developed, demonstrating its beam steering capability by changing the scanning angle between 0°, −25° and +15° with three different voltage distributions. The antenna array is well matched throughout the complete W-band with a input reflection below −10 dB. The measured antenna gain is between 11.5 to 9.1 dBi at 85 GHz accompanied with a side lobe level between −12 to −7 dB, depending on the steering configuration.

INDEX TERMS Phased array, millimeter wave devices, microwave liquid crystal, dielectric waveguide.

I. INTRODUCTION

Millimeter wave and terahertz frequencies gained more and more research interest as they can be used for high data rate wireless radio links or radar imaging. Due to the high transmit frequencies, large absolute bandwidths are available, which offer high data rates. Furthermore, a large amount of unused frequency bands are available. At these frequencies, dielectric waveguides (DW) came into focus of research and development due to their numerous advantages in comparison to conventional metallic waveguides. On one hand, they offer a low-loss propagation since ohmic losses are avoided and on the other hand they can be fabricated at low costs using e.g. 3D printing or injection molding. Furthermore, as they are fully dielectric, DWs are very lightweight.

DWs and corresponding rod antennas have been presented as suitable antenna elements for phased arrays in [1]–[4]. However, in these works only non-reconfigurable arrays have been presented, focusing more on feeding network designs and evaluation of the overall antenna array performance. Nevertheless, it could be shown in these papers that well performing antenna arrays can be designed using DWs. For reconfigurability and beam steering, phase shifters are needed in order to adjust the phase shift distribution along the antenna elements. Several technologies based on the functional material liquid crystal (LC) and micro-electro-mechanical systems (MEMS) are available as possible solutions for DW phase shifters. In [5] and [6] high impedance surfaces (HIS) based on MEMS structures are presented, which are placed close to a high permittivity DW. With change of the applied voltage to the MEMS, the surface impedance of the HIS changes, and therefore, the propagation constant of the DW. However, MEMS suffer from wear-out failures due to their mechanical moving parts and their fabrication is difficult. Furthermore, the distance between HIS structure and the DW has a large impact to the phase difference and only little

The associate editor coordinating the review of this manuscript and approving it for publication was Guan-Long Huang.

spatial displacement is allowed without affecting the phase shifter performance too much [6]. As alternative to MEMS based tunable HIS, carbon nanotubes are used in [7] and [8] to control the propagation constant of the DW. In these works the carbon nanotube layer is optically controlled by applying different light intensities. However, this technology lacks of tunability, and therefore, just small phase shifts and low Figures-of-Merit (FoM) are possible.

Microwave LC based phase shifters for DWs have been presented as subwavelength fiber in [9] and as classical dielectric waveguide or also called step-index fiber in [10]. In these works, LC is placed as a core material inside the DW and the LC's anisotropy is used to continuously adjust the phase shift with electric and magnetic biasing fields. Although both, the MEMS as well as the LC phase shifters, are electrically tunable, the LC phase shifters have the advantage that no wear out failures can occur and the fabrication is comparably simple. Furthermore, LC shows low losses, which results in a high FoM of around 100°/dB [10], and it stays low loss even in the terahertz region [11]. The main disadvantage is on one hand the relatively slow tuning speed or response time, which occurs due to the reorientation of the LC molecules. Challenging is also the proper sealing of the LC cavity in the DW to avoid leakage.

Based on the work presented in [9], LC filled DWs are used for the first time as phase shifter elements for an 1×4 rod antenna array at W-band. Using a waveguide feeding network, LC filled subwavelength fibers are directly connected to the rod antenna elements to achieve beam steering.

This paper is divided as follows. Section II introduces LC as tunable material. Section III, then, presents the phase shifter design and Section IV the design of the phased array including the feeding network as well as the electric biasing. A proof-of-concept with the corresponding measurements are given in Section IV. At the end, a conclusion is given in Section V.

II. MICROWAVE LIQUID CRYSTAL FUNDAMENTALS

The term liquid crystal describes a special material class, which shows the characteristic of a fluid and that of a crystal at the same time. LC can flow like a liquid but its rod-like molecules maintain a certain orientational order like in a crystal, which is why LC shows also birefringence and anisotropy. The anisotropy is described by $\Delta\varepsilon_r = \varepsilon_{r,\parallel} - \varepsilon_{r,\perp}$ with the permittivity of the long $\varepsilon_{r,\parallel}$ and short $\varepsilon_{r,\perp}$ axis of the LC molecule, respectively.

In order to achieve a macroscopical description of LC, the director $\vec{n}$ is used, which is defined as a unit volume element aiming towards the average direction of the LC molecules inside this volume element. With the direction of $\vec{n}$, two different extreme states of the permittivitiy with respect to an applied RF field are possible. If $\vec{n}$ is perpendicular oriented to the RF field, the LC shows a permittivity of $\varepsilon_{r,\perp}$ and a permittivity of $\varepsilon_{r,\parallel}$ if the RF field is parallel to $\vec{n}$. In between these two extreme states, a continuous tuning can be achieved by applying external quasistatic electric or magnetic fields, since the LC molecules tend to align themselves parallel to the field lines. For deeper understanding of LC used for microwave applications, we refer to [12]. The LC mixture used in this work is the new GT7-29001, specifically synthesized for microwave applications by Merck KGaA. It shows a permittivity range from $\varepsilon_{r,\perp} = 2.45$ to $\varepsilon_{r,\parallel} = 3.53$ with a dissipation factor between $\tan\delta_\perp = 0.0116$ and $\tan\delta_\parallel = 0.0064$ at 19GHz. The measured values are provided by Merck KGaA. In [11], it is shown that microwave LCs keep their good material properties up to several terahertz. Furthermore, a 60GHz resonator setup for LC characterisation is presented in [13]. Within this work, the good and nearly constant material properties at higher frequencies are confirmed. This behavior of the material parameters is also expected for the used LC GT7-29001.

III. PHASE SHIFTER DESIGN

The principle design of the phase shifter was initially proposed in [9] and is used for a tunable fully dielectric SPDT in [14]. In these works, the DW was designed as subwavelength fiber consisting just of a single dielectric core. The main characteristic of such subwavelength fibers is that decaying evanescent fields are present in the air surrounding the DW. By inserting LC in the fiber, tunability is achieved as the tunable permittivity is used to change the propagation constant of the DW. Based on the previous work, we developed the phase shifter shown in Fig. 1. The fiber is made out of the crosslinked plastic Rexolite with a permittivity of $\varepsilon_r = 2.53$ and a dissipation factor of $\tan\delta = 0.0006$ at 100GHz [15]. In comparison to [9], [14], the LC cross section is significantly increased to achieve a higher tunability. The fiber has a quadratic shape of $1.8 \times 1.8\,\text{mm}^2$ with a non-quadratic LC cavity of $1.4 \times 1.2\,\text{mm}^2$ inside the fiber. The rectangular shape of the LC cavity was chosen to ensure a better polarization stability. In order to ensure a sufficient mechanical stability 0.2mm and 0.3mm thin Rexolite walls are chosen, which is a good trade off to meet the limitations in the later CNC milling fabrication.

The design process was done using CST Studio Suite simulations. The length of the LC section was chosen with a large margin of the phase shift for the later application in the phased array, in order to reduce the complexity of the electric biasing system. To simplify the biasing network, only two biasing electrodes per phase shifter are used to control the LC orientation from perpendicular towards parallel orientation. This is possible, because with zero bias most LC molecules in the DW are naturally more perpendicular oriented without any additional alignment layer such as a polyimid film in displays. However, the tuning effectiveness, which describes quantitatively how much of the material's tunability can be utilized by a proposed device layout goes down to some extend compared to perfect perpendicular orientation of almost all LC molecules in the zero biasing state. This means, the length of the LC tuned DW section has to be longer to achieve the desired 360° phase shift needed for the phased array.

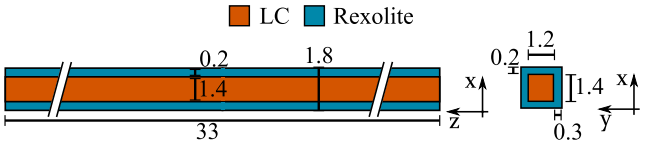

FIGURE 1. Cross section of the subwavelength fiber phase shifter used in this work. All dimensions are given in mm.

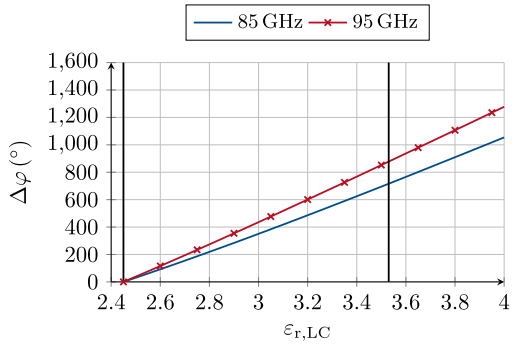

FIGURE 2. Simulated phase shift over permittivity of the microwave LC GT7-29001 at two frequencies. The simulated phase shifter is depicted in Fig. 1. Each simulated phase shift is individually normalized.

The simulated behavior of the differential phase over permittivity of the LC is depicted in Fig. 2 for 85 and 95GHz, respectively. If the anisotropy of $\Delta\varepsilon_r = 1.08$ can be fully exploited, a maximum phase shift of 680° can be achieved at 85GHz, whereas with a reduced tuning effectiveness, e.g. with an effective anisotropy of $\Delta\varepsilon_r = 0.6$ only, the maximum phase shift would be decreased down to 360°. Despite the simplified biasing network, a length of 33mm of the phase shifter is therefore suitable for a phased array.

A. FABRICATION AND MEASUREMENT OF THE PHASE SHIFTER

The phase shifters are assembled of two milled Rexolite halves, which are glued together using a ultraviolet glue. On the front side, a filling channel is considered to fill in the LC with a syringe. After filling in the LC, the channel is sealed with epoxy glue. Fig. 3a) shows a fabricated phase shifter. As can be seen, connection clips are considered for the assembly in the phased array. Several phased shifter have been assembled and are individually characterized at first, both with magnetic and electric biasing. The used measurement setups for magnetic and electric biasing are shown in Figs. 3b) and c), respectively. Within this measurement setup, WR10 horn-like transitions are used, similar to the one used in [10] and [14] to connect the phase shifters to a Keysight PNA, including W-band extension modules from Anritsu.

The magnetic biasing was achieved by means of rare earth magnets, which apply a magnetic flux density of 0.2T. For electric biasing a 1kHz rectangular signal, which was amplified by a voltage amplifier to 500V, was applied. As can be seen in Fig. 3, the rare earth magnets were hold in position

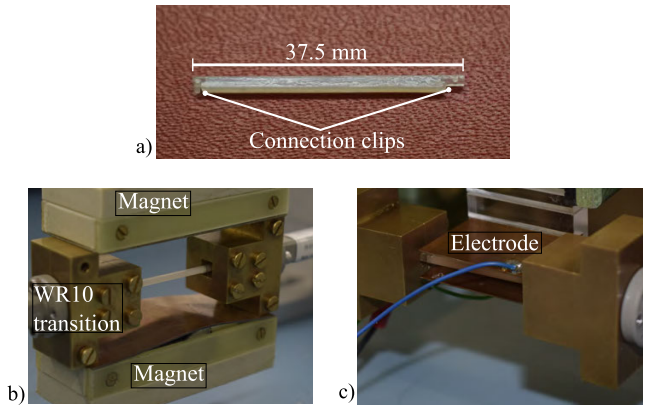

FIGURE 3. a) Photograph of the assembled subwavelength fiber phase shifter. Measurement setup of b) magnetic characterization and c) electric characterization of the phase shifter, respectively.

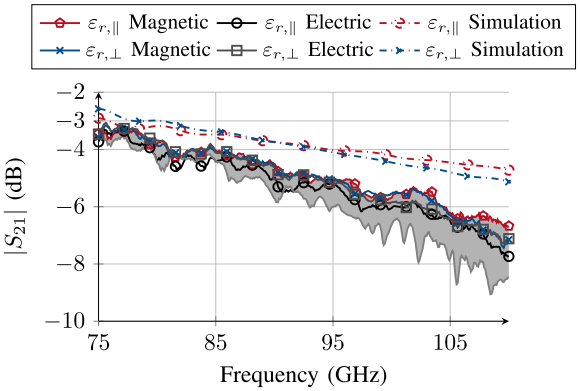

FIGURE 4. Comparison of measured and simulated S-Parameter of a phase shifter. Shown is the best result, while in grey, the range of all measured phase shifters for both principle orientations $\varepsilon_{r,\perp}$ and $\varepsilon_{r,\parallel}$ is depicted.

by the WR10 transitions, while the electrodes were mounted on a mechanical fixture with a distance of 6mm between each other. For reorientation of the LC, the magnets and the electrodes were rotated by hand.

The phase shifter performance regarding the simulated and measured scattering parameter $|S_{21}|$ is shown in Fig. 4. In this plot, the best results as well as the range of all measured phase shifters are shown. Two characteristics of the phase shifters in the measurement can be observed. First, 1dB more loss occurs in comparison to the simulation. Second, although the perpendicular LC orientation is more lossy than the parallel orientation, the $|S_{21}|$ is nearly the same for both LC orientations. This can be explained with the higher field confinement in the case of a parallel LC-orientation inside the fiber, which is due to the higher permittivity. With lower permittivity, the amount of evanescent field outside the fiber increases, and hence, the RF wave propagates more in air. Therefore, the resulting total loss of perpendicular and parallel LC orientation is nearly the same.

The additional loss comes from the splice and the used glues, which were not included in the simulation as the dissipation factors of the glues are unknown at these high

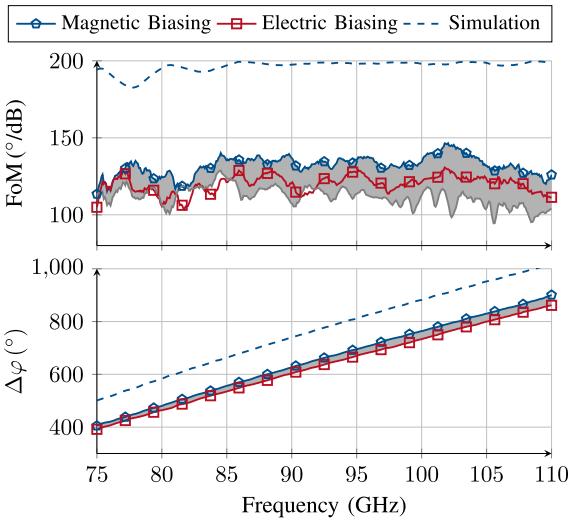

FIGURE 5. Simulated and extracted FoM as well as differential phase shift using both extreme LC orientations. In grey, the range of all measured phase shifters is depicted.

frequencies. Furthermore, the gluing process leads to an uncertainty of the fiber dimensions. The resulting thickness of the phase shifter is increased by 50 to 100μ m and varies between each phase shifter as they are assembled by hand. Furthermore, the dimension changes along the DW phase shifter. Some glue residues at the outer surface or can also flow inside the LC cavity during gluing. This variation of the dimension leads to additional radiation of the DW, especially at high frequencies. Each discontinuity excites radiation modes, which increases the loss. Therefore, each assembled phase shifter showed slightly different results with respect to $|S_{21}|$. Especially at higher W-band frequencies, the measured $|S_{21}|$ of the phase shifters is more differing. This indicates that radiation occurs due to the discontinuities, as the smaller wavelength is more sensitive to the assembly tolerances. Fig. 5 depicts the simulated and the extracted FoM from measurements as well as the maximum differential phase shift. The FoM is defined as the ratio of maximum differential phase shift and maximum insertion loss, given by

$$\mathrm{FoM} = \frac{\Delta\varphi_{\max}}{\mathrm{IL}_{\max}}. \tag{1}$$

Due to the additional loss and less phase shift, the simulated FoM of 200°/dB is not achieved by the realized phase shifter. Nevertheless, the FoM shows an average of 140°/dB for magnetic and 130°/dB for electric biasing in the frequency range from 85 to 110GHz. The differential phase shift varies between 400° to about 900° for both biasing schemes. Generally, both the FoM and differential phase shift with electric biasing is lower than for magnetic biasing, since the tuning effectiveness can never be fully exploited with electric biasing due anchoring effects of the plastic wall. Furthermore, the metallic WR10 transition can disturb the static biasing field as it acts as a floating electrode. Therefore, the E-field is less homogeneous than the magnetic field and less phase shift can be achieved.

TABLE 1. Comparison of W-band dielectric waveguide phase shifters with this work.

Waveguide	Technology	FoM (°/dB)	°/mm	f (GHz)	Reference
Subwavelength fiber	MEMS	104	11	80	[5]
Subwavelength fiber	Nanotubes	4	0.75	75-110	[7]
Subwavelength fiber	Nanotubes	3	2	220-330	[8]
Subwavelength fiber	LC	60	5	90-110	[14]
Subwavelength fiber	LC	42	4.6	90-110	[9]
Dielectric waveguide	LC	100	18	75-110	[10]
Subwavelength fiber	LC	130	22	85-110	This work

The measured differential phase shift shows a large discrepancy of around 120° in comparison to the simulation. This is because the LC is not perfectly aligned as assumed in the simulation and the modelling of the LC's permittivity in the simulation is not accurate. In the latter case, permittivity values at 100GHz were not available at the time of the design process. Furthermore, residual air bubbles occured during the assembly which affects the possible phase shift.

A comparison of dielectric waveguide phase shifters is given in Table 1. Based on this table, it can be observed that the proposed phase shifter in this work set a new benchmark at W-Band frequencies.

IV. PHASED ARRAY DESIGN

With the proposed phase shifter design, a phased array was designed with the schematic shown in Fig. 6. It consists of, **(A)** a cascaded E-plane power divider, **(B)** dielectric taper, which are inserted into the waveguide, **(C)** horn-like transitions from waveguide to DW, **(D)** the phase shifter section and **(E)** the rod antenna elements. As a trade-off of small distances between the antenna elements and the assembly of the antenna, a distance of 2.8mm ($\approx 0.8\lambda_0$ @ 85GHz) between the antennas was chosen.

As most suitable antenna type for DW, rod antennas were chosen [16], as they can be directly connected to the DW phase shifters. They belong to aperture antennas, since their taper increases the size of the E-field distribution at the taper end, and therefore, the antenna gain. In this work, the taper is considered on all sides of the rod antenna. With a taper length of 8mm, a suitable length was found in the simulations with a simulated average half power beam width of 45°, see Fig. 9.

The cross section of the designed phased array is shown Fig. 6.

A. FEEDING NETWORK

For the feeding of the four phase shifters and antenna elements, a corporate waveguide E-plane power divider network was designed. By inserting a thin metallic wall in the center of

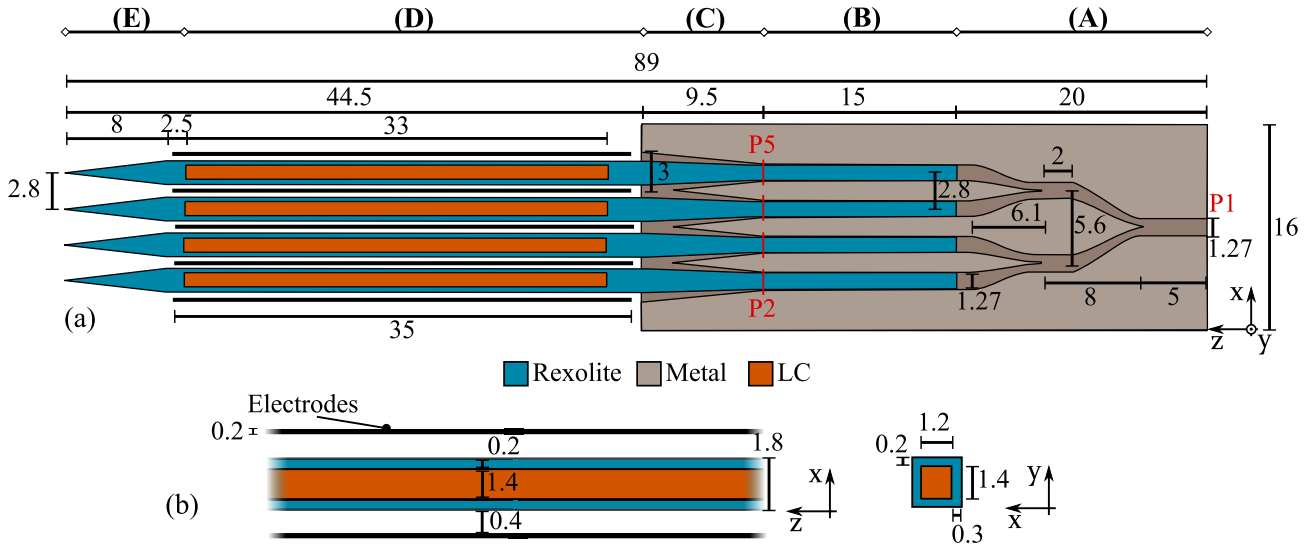

FIGURE 6. Cross section of the proposed rod antenna array. a) (A) Cascaded E-plane power divider. (B) Dielectric taper. (C) Horn-like transition from metallic waveguide to DW. (D) Phase shifter section. (E) Rod antennas. In red, the port definition used in CST Studio Suite (P1,...,P5) is given. b) Detailed view of the phase shifter section including the electrodes. All dimensions are given in mm.

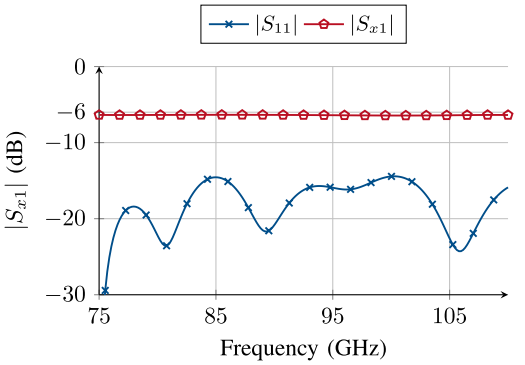

FIGURE 7. Simulated S-parameter results of the four-way power divider with the port definition depicted in Fig. 6. $x = 2, 3, 4, 5$.

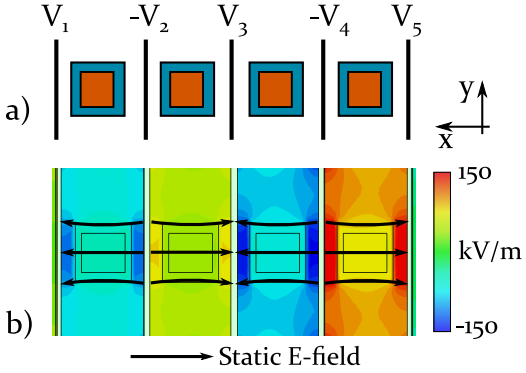

FIGURE 8. a) Principle sketch of the electric biasing network consisting of five electrodes. b) Simulated E-field distribution for a potential distribution of $V_1 = 80V$, $V_2 = 80V$, $V_3 = 30V$, $V_4 = 170V$ and $V_5 = 70V$.

the waveguide, the wave is separated. By using gentle taper and bends, which should be around three wavelengths long with respect to the WR10 dimension, broadband matching can be achieved. For the the excitation of the DW phase shifters, a horn-like transition was used similar to the one in [9], [10], [14]. With a horn size of $3 \times 3\text{mm}^2$, a good trade-off between good transition and compactness was found. With this horn-like structure, a transition from dielectrically filled metallic waveguide to DW is possible. For proper matching, a taper of 9mm of the inserted dielectric is considered. Furthermore, the metal walls of the waveguide are tapered towards a smaller cross-section of $1.27mm \times 1.8mm$ to avoid a higher order mode propagation. With the port definition depicted in Fig. 6, simulation results of the S-parameters can be found in Fig. 7. In this simulation, the dielectric taper as well as the H-plane divider itself is considered including also the losses of Rexolite and brass, respectively. The simulation resulted in an equal power split of 6dB with additional 0.3dB loss throughout the whole W-band and a $|S_{11}|$ better than -15dB.

B. ELECTRIC BIASING NETWORK

The principle design of the electric biasing system is presented in Fig. 8a). With the antenna distance of 2.8mm, the resulting distance between DW and electrode is around 0.4mm. As mentioned in Sec. III, only the LC orientation from the initial perpendicular state to the parallel state will be controlled by external electric fields in order to reduce the biasing complexity. Thus, in total five electrodes, and therefore, five potentials are necessary for the electric biasing. In comparison, for a fully electric biasing, 13 electrodes would be needed.

The applied voltages are connected alternating to either a positive or negative voltage to achieve a homogeneous static E-field distribution inside the LC core. This is confirmed by a CST Studio Suite simulation of the static E-field. The simulation result for an arbitrarily chosen potential distribution is presented in Fig. 8b). In this simulation, the E-field stays homogeneous inside the LC core for every applied potential distribution.

As it was discussed already in [1] and [3], strong coupling effects can occur between two closely spaced adjacent DWs. Due to the evanescent fields, coupling of the EM wave occurs even for relatively large distances between DWs of around 1mm. Due to the inserted metallic electrodes, coupling is significantly reduced as the DWs are shielded by the electrodes. However, only small tolerances of the electrode placement are allowed because of the strong interaction of the propagating RF wave and the electrodes. With a change of the distance between electrodes and DW, the propagation constant changes. This effect could lead to an variation of the phase shift and should be kept as small as possible.

C. SIMULATION OF THE PHASED ARRAY

In addition, the single antenna pattern in Fig. 9 of the antenna in the array is included. It can be seen that the nearfield coupling between the antenna elements is only visible for lower frequencies. However, only a pattern degradation of 3dB is visible. The single antenna was excited in the simulations at the position of the dielectric taper inside the WR10 waveguide. The neighboring unused antenna ports are matched. Simulations show that the coupling between the excited antenna and the neighboring antennas is below −20dB. The beam steering capabilities of the designed phased array were investigated first in a simulation, changing the permittivity value of the LC in each phase shifter individually. As discussed in Sect. III, the phase shift is linearly dependent of the permittivity, and therefore, three different progressive changes of the permittivity between each phase shifter were investigated. The lowest permittivity is $\varepsilon_{r,\perp}$. Starting from one of the outer phase shifters, a phase shift is induced for each antenna element, and therefore, the beam is steered. The result of these investigations is given in Fig. 10 for a progressive permittivity change of $\Delta\varepsilon_{r,LC} = 0$, $\Delta\varepsilon_{r,LC} = -0.1$ and $\Delta\varepsilon_{r,LC} = 0.2$, which leads to radiation towards 0°, +15° and −25°, respectively. Although the used LC GT7-29001 has a higher anisotropy, this value was used to have enough margin for the later measurement. At 95GHz high side lobes occur due to the relatively large antenna element spacing. The simulated H-plane is depicted in Fig. 11.

D. ASSEMBLED PHASED ARRAY AND PHASE CHARACTERIZATION

The electrodes are realized by laser cut 200μ m thin metal plates, which are soldered to FR-4 PCBs. The assembled phased array is shown in Fig. 12. It consists of the power divider network realized in split block technology, the DW phase shifters, the rod antennas and the electrodes connected to FR-4 PCBs. As can be seen, the PCBs are directly mounted on the split block to keep the electrodes in position. For better adjustment, small Rohacell pieces can be inserted between the electrodes and DW phase shifters. The measured performance of the phase shifters presented in Sect. III is not sufficient for the application in the phased array, as the phase response with respect to the applied voltage is not known. The reason can be found in the changed electrode distances,

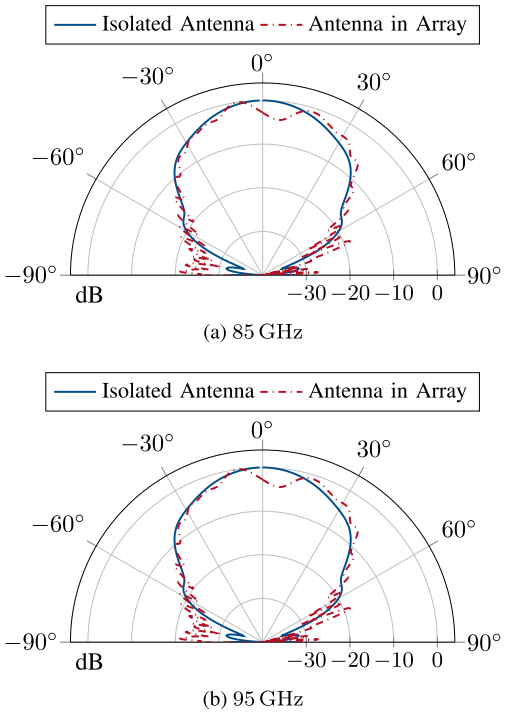

FIGURE 9. Simulated E-plane antenna pattern of a single rod antenna element. The pattern of the single antenna as well as the antenna in the array is shown. Each pattern is individually normalized.

and therefore, a different phase shift characteristic. Since the electric biasing is limited to the parallel LC orientation, each phase shifter has to be characterized as the unbiased state is not well defined regarding the LC orientation. Surface anchoring effects between the Rexolite and the LC molecules, due to the surface roughness, change the unbiased state. For the phase difference over voltage characterization, the rod antennas were dismounted and each single phase shifter was measured consecutively with an additional WR10 to DW transition. Two pairs of phase shifters, which were fabricated with two different milling tools, were measured. The result of this measurement is shown in Fig. 13. Noticeable is that less voltage must be applied to achieve a phase shift compared to Sect. III due to the smaller electrode distances. It can be observed that the two pairs resulted in two different phase characteristics. This is a hint, that the initial LC orientation in the unbiased state is very sensitive to the surface roughness of the milled Rexolite. However, a phase shift of at least 250° can be achieved. Although the biasing voltage was increased up to 200V, a saturation of the phase shift can be observed for every phase shift at around 100V and only a marginally increase of phase shift occurs with higher voltage. The switching time, which is the time the LC needs to orientate itself from the no-bias state to the fully parallel orientation is 17 seconds for 200V. A similar switching time is expected for the perpendicular orientation, but cannot be measured with this setup due to the simplified electric biasing network. The LC reorientation towards the no-bias state is achieved within a few minutes after the voltage is switched off.

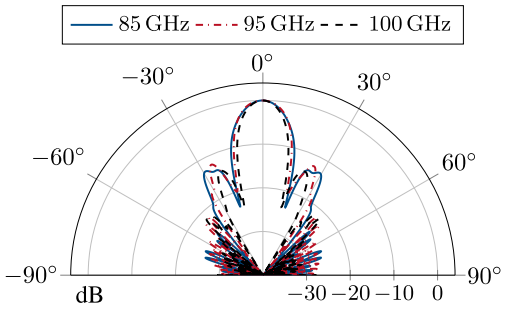

(a) Angle of radiation of 0°

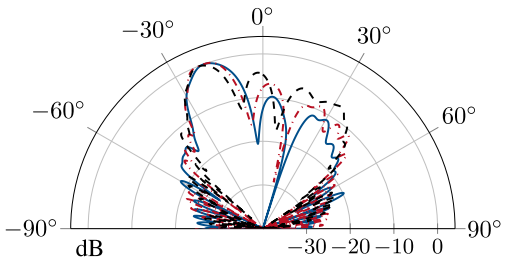

(b) Angle of radiation of −25°

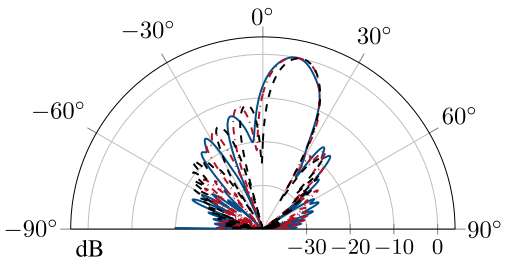

(c) Angle of radiation of +15°

FIGURE 10. Simulated E-plane antenna pattern at three frequencies. Three different progressive permittivity changes of the LC, $\Delta\varepsilon_{r,LC} = 0$, $\Delta\varepsilon_{r,LC} = 0.2$ and $\Delta\varepsilon_{r,LC} = -0.1$, are used for each configuration. Each pattern is individually normalized.

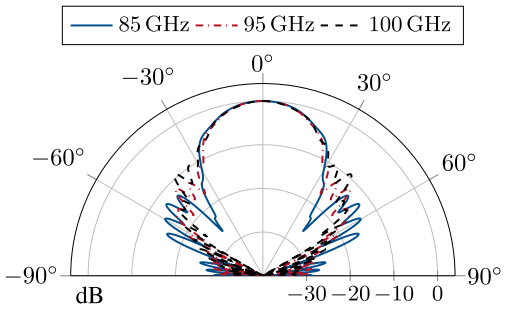

FIGURE 11. Simulated H-plane antenna pattern with the antenna array pointing towards 0°. Each pattern is individually normalized.

E. ANTENNA MEASUREMENTS

The first measurement, which was conducted with the complete phased array, was the measurement of the matching $|S_{11}|$. The comparison of simulation and measurement is depicted in Fig. 14. It can be observed that the $|S_{11}|$ is below −10dB over the whole frequency range. Furthermore, we observed in the measurement that the matching is nearly independent of the biasing.

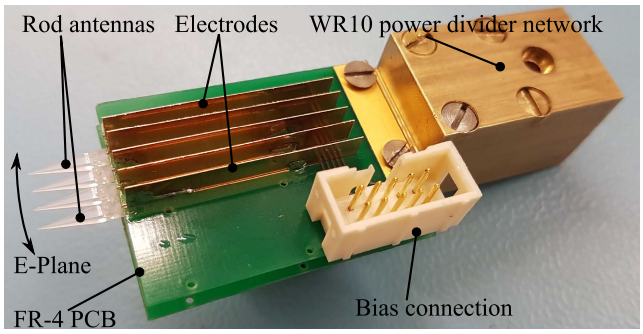

FIGURE 12. Photograph of the assembled phased array antenna.

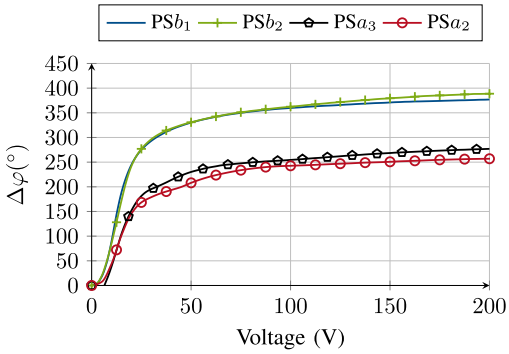

FIGURE 13. Measured phase shift over bias voltage at 85GHz. Two pairs of two different milling processes (a_i and b_i) were measured. Each phase shift is individually normalized.

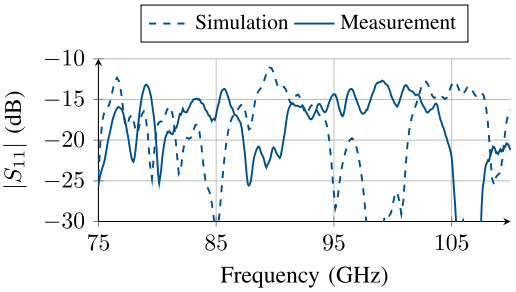

FIGURE 14. Comparison of simulated and measured $|S_{11}|$ of the complete phased array. The matching is nearly independent of the biasing states and stays always below −10dB.

In order to evaluate the beam steering mechanisms of the phased array, three distinct voltage distributions, according to Fig. 13 and Tab. 2 were defined at 85GHz. The voltage distributions lead to a radiation towards 0°, −25° and +15°. For the 0° radiation in broadside direction, each phase shifter was configured to compensate the phase shift due to the different zero-biasing states. The different initial phase shifts due to the different zero-bias of each phase shifter were included in the beam steering configurations.

The pattern measurements were conducted by using the flexible waveguide assembly from Spinner [17], which is connected to the turntable. Due to mechanical limitations, only a rotation of ±65° of the turntable is possible. The measurements of the non-steerable radiation in H-plane as well as the three different configurations for beam steering in

TABLE 2. Voltage distribution for three different angles of radiation for 85GHz.

Angle of radiation	$\|V_1\|$	$\|V_2\|$	$\|V_3\|$	$\|V_4\|$	$\|V_5\|$
0°	27 V	14 V	10 V	13 V	13 V
−25°	0 V	28 V	18 V	2 V	12 V
+15°	24 V	12 V	12 V	40 V	187 V

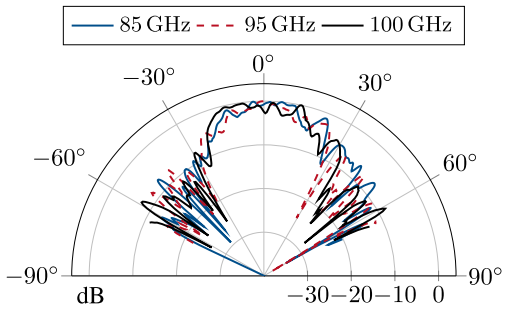

FIGURE 15. Individually normalized measured antenna pattern in the H-plane. In this measurement, the beam in the E-plane was configured to radiate in a direction of 0°.

the E-plane are depicted in Fig. 15 and Fig. 16, respectively. The effect of the different applied voltage, and therefore, different phase shifts is well observable. Each voltage configuration shows a different beam steering behavior, with a side lobe level in a range of −12 to −7dB at 85GHz. The antenna gain was measured with a 22dBi standard gain horn and is 11.5dBi for the non-steered radiation towards 0° and decreases to 9.1dBi for steering towards −25°, both measured at 85GHz. At 100GHz it can be observed that the beam width is wider, because the phase shifts were chosen for 85GHz. In comparison to simulations, the gain at 85GHz is around 1.5dB lower, mainly based on the unknown loss of the glue and the not available LC parameters at these high frequencies.

Although the beam steering capability of the proposed antenna array is successfully proven, a large ripple level can be observed in the radiation patterns. This becomes even more evident, comparing the measurement with the simulation, see Fig. 10. The reason are the metal electrode plates and tolerances in their positions, which lead to diffraction effects at the end of each phase shifter section, which degrades the antenna pattern. This is also visible as ripples in the E-plane measurement in Fig. 15. The assembly of the single parts, such as the phase shifters, taper and rod antennas, lead to further spatial displacement. Although small Rohacell pieces were used to ensure a proper electrode placement, the DW phase shifters are very sensitive to small spatial deviations. This causes unwanted radiation which increases the ripple level in the antenna patterns.

In order to understand the effect of the spatial displacement, a simulation is perfomed. Within this simulation, several tolerances of the electrodes, the phase shifters as well as the rod antennas are considered. The displacements of the single components have been chosen arbitrarily, with a maximum change of the position of 5% in comparison to the ideal position. The result of this simulation is shown

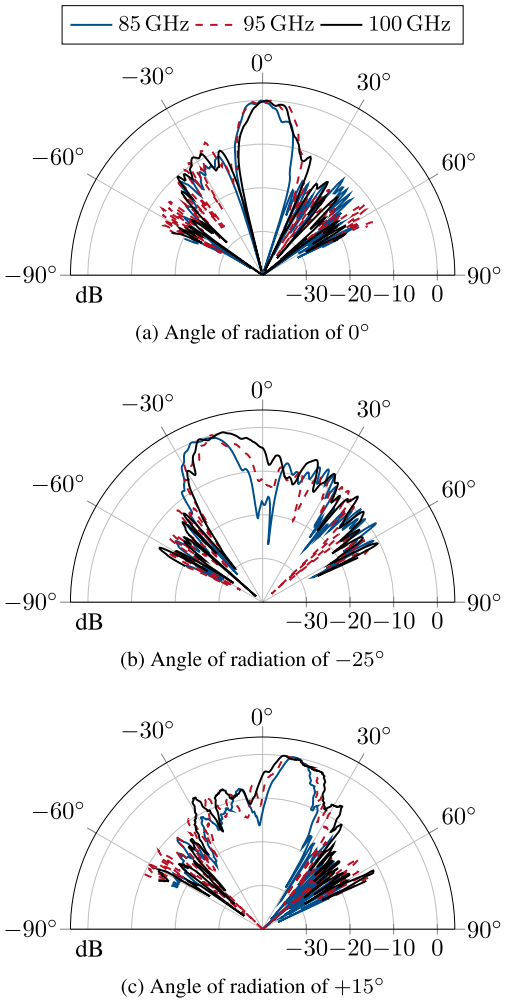

FIGURE 16. Measured E-plane antenna pattern at three frequencies for three different angle of radiations. Each pattern is individually normalized.

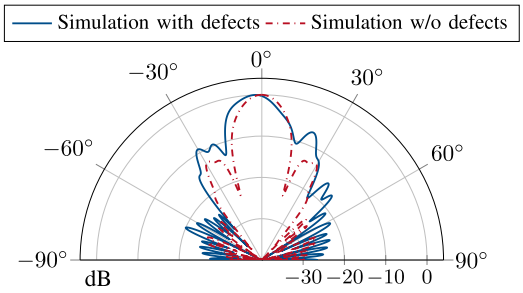

FIGURE 17. Simulation of the antenna with defects caused by assembly tolerances. For comparison the pattern of ideal antenna array is included.

in Fig. 17. It can be observed that the antenna pattern is degraded, the SLL is increased and the main beam direction deviates from the ideal broadside direction. However, the high ripple level is not visible in the simulation.

V. CONCLUSION AND OUTLOOK

For the first time, a continuously electrical steerable phased array at W-band frequencies is presented using microwave liquid crystals (LC). LC filled dielectric waveguides (DW)

mad out of Rexolite are used as phase shifter elements connected to rod antennas as antenna element. A 1×4 array was designed including also a waveguide power divider network consisting of cascaded E-plane power divider. The phase shifters, which were designed as subwavelength fibers, achieved a maximum phase shift of 400° to 900° from 75GHz to 110GHz accompanied with an insertion loss between 3.5 to 7.8dB. This results in an average Figure-of-Merit (FoM) of 130°/dB, with a maximum FoM of 145°/dB at 102.5GHz. For electric biasing of the LC, a simplified electrode biasing network was developed, consisting of five electrodes, where the initial orientation of the LC's is given by the surface roughness of the Rexolite container only. This leads to a reduced tuning effectiveness, since the LC molecules are not all perpendicular to the RF field, and hence, differential phase shift. Challenging is also the proper alignment and placement of the single electrodes as this affects the DW phase shifters. In addition, radiation due to small spatial deviations of the electrodes can degrade the antenna pattern. Disadvantageous, is also the assembly process of the single parts, as the phase shifters as well as the complete antenna array is sensitive to fabrication tolerances. Despite the simplified electrode biasing network, beam steering is demonstrated, which is shown with three different configurations, resulting in radiation towards 0°, −25° and +15°. Depending on the radiation angle, the side lobe level is between −12 and −7dB with a measured antenna gain ranging from 11.5 to 9.1dBi at 85GHz.

In future, the array can be designed fully dielectric as such non-steerable rod antenna arrays are proposed in [3] and [4]. With this approach, very lightweight antenna arrays could be designed, since the waveguide power divider network can be omitted. This presented design technique allows also an integrated design, resulting in a better fabrication tolerances, and therefore, less radiation. Furthermore, a more compact design can be achieved with a fully electric biasing scheme, which fully exploits the tuning effectiveness, and hence, differential phase shift, so that the phase shifter can be shorter. A reduction of the antenna element spacing can be achieved by using materials with a higher permittivity [18]. This decreases the DW dimensions, and hence, a closer spacing can be realized without affecting the coupling.

ACKNOWLEDGMENT

The authors would like to thank CST AG, Darmstadt, Germany, for providing CST Microwave Studio and Merck KGaA, Darmstadt, Germany, for providing the LC mixtures.

REFERENCES

[1] J. P. Pousi, D. V. Lioubtchenko, S. N. Dudorov, and A. V. Raisanen, "High permittivity dielectric rod waveguide as an antenna array element for millimeter waves," *IEEE Trans. Antennas Propag.*, vol. 58, no. 3, pp. 714–719, Mar. 2010.

[2] A. Rivera-Lavado, L.-E. García-Muñoz, A. Generalov, D. Lioubtchenko, K.-A. Abdalmalak, S. Llorente-Romano, A. García-Lampérez, D. Segovia-Vargas, and A. V. Räisänen, "Design of a dielectric rod waveguide antenna array for millimeter waves," *J. Infr., Millim., THz. Waves*, vol. 38, no. 1, pp. 33–46, Jan. 2017.

[3] R. Reese, M. Jost, M. Nickel, E. Polat, R. Jakoby, and H. Maune, "A fully dielectric lightweight antenna array using a multimode interference power divider at W-band," *IEEE Antennas Wireless Propag. Lett.*, vol. 16, pp. 3236–3239, 2017.

[4] R. Reese, H. Tesmer, M. Jost, E. Polat, M. Nickel, R. Jakoby, and H. Maune, "A compact two-dimensional power divider for a dielectric rod antenna array based on multimode interference," *J. Infr., Millim., THz. Waves*, vol. 39, no. 12, pp. 1185–1202, Dec. 2018.

[5] D. Chicherin, M. Sterner, J. Oberhammer, S. Dudorov, D. Lioubtchenko, A. J. Niskanen, V. Ovchinnikov, and A. V. R Räisänen, "MEMS based high-impedance surface for millimetre wave dielectric rod waveguide phase shifter," in *Proc. 40th Eur. Microw. Conf.*, Sep. 2010, pp. 950–953.

[6] D. Chicherin, M. Sterner, D. Lioubtchenko, J. Oberhammer, and A. V. Räisänen, "Analog-type millimeter-wave phase shifters based on MEMS tunable high-impedance surface and dielectric rod waveguide," *Int. J. Microw. Wireless Technol.*, vol. 3, no. 5, pp. 533–538, Oct. 2011.

[7] D. V. Lioubtchenko, I. V. Anoshkin, I. I. Nefedova, J. Oberhammer, and A. V. Räisänen, "W-band phase shifter based on optimized optically controlled carbon nanotube layer," in *IEEE MTT-S Int. Microw. Symp. Dig.*, Jun. 2017, pp. 1188–1191.

[8] S. Smirnov, I. V. Anoshkin, D. V. Lioubtchenko, and J. Oberhammer, "Millimeter wave phase shifter based on optically controlled carbon nanotube layers," in *Proc. 43rd Int. Conf. Infr., Millim., THz. Waves (IRMMW-THz)*, Sep. 2018, pp. 1–2.

[9] M. Jost, R. Reese, C. Weickhmann, C. Schuster, O. H. Karabey, H. Maune, and R. Jakoby, "Tunable dielectric delay line phase shifter based on liquid crystal technology for a SPDT in a radiometer calibration scheme at 100 GHz," in *IEEE MTT-S Int. Microw. Symp. Dig.*, May 2016, pp. 1–4.

[10] R. Reese, M. Jost, H. Maune, and R. Jakoby, "Design of a continuously tunable W-band phase shifter in dielectric waveguide topology," in *IEEE MTT-S Int. Microw. Symp. Dig.*, Jun. 2017, pp. 180–183.

[11] C. Weickhmann, R. Jakoby, E. Constable, and R. A. Lewis, "Time-domain spectroscopy of novel nematic liquid crystals in the terahertz range," in *Proc. 38th Int. Conf. Infr., Millim., THz. Waves (IRMMW-THz)*, Sep. 2013, pp. 1–2.

[12] H. Maune, M. Jost, R. Reese, E. Polat, M. Nickel, and R. Jakoby, "Microwave liquid crystal technology," *Crystals*, vol. 8, p. 9, Sep. 2018.

[13] E. Polat, R. Reese, H. Tesmer, S. Schmidt, M. Spaeth, M. Nickel, C. Schuster, R. Jakoby, and H. Maune, "Characterization of liquid crystals using a temperature-controlled 60 GHz resonator," in *Proc. IEEE MTT-S Int. Microw. Workshop Ser. Adv. Mater. Process. (IMWS-AMP)*, Jul. 2019, pp. 19–21.

[14] M. Jost, R. Reese, M. Nickel, H. Maune, and R. Jakoby, "Fully dielectric interference-based SPDT with liquid crystal phase shifters," *IET Microw., Antennas Propag.*, vol. 12, no. 6, pp. 850–857, May 2018.

[15] G. L. Friedsam and E. M. Biebl, "Precision free-space measurements of complex permittivity of polymers in the W-band," in *IEEE MTT-S Int. Microw. Symp. Dig.*, vol. 3. Jun. 1997, pp. 1351–1354.

[16] S. Kobayashi, R. Mittra, and R. Lampe, "Dielectric tapered rod antennas for millimeter-wave applications," *IEEE Trans. Antennas Propag.*, vol. 30, no. 1, pp. 54–58, Jan. 1982.

[17] H.-U. Nickel and J. Zovo, "Novel flexible dielectric waveguide for millimeter and sub-millimeter frequencies—Design and characterization," in *Proc. 84th ARFTG Microw. Meas. Conf.*, Dec. 2014, pp. 1–4.

[18] R. Reese, H. Tesmer, E. Polat, M. Jost, M. Nickel, R. Jakoby, and H. Maune, "Fully dielectric rod antenna arrays with high permittivity materials," in *Proc. 12th German Microw. Conf. (GeMiC)*, Mar. 2019, pp. 13–16.

ROLAND REESE (S'17) was born in Darmstadt, Germany, in 1990. He received the B.Sc. and M.Sc. degrees in electrical engineering from Technische Universität Darmstadt, in 2013 and 2015, respectively, where he is currently pursuing the Ph.D. degree with the Institute for Microwave Engineering and Photonics with a focus on new devices and antennas in the millimeter wave range.

ERSIN POLAT was born in Alzenau, Germany, in 1991. He received the B.Sc. and M.Sc. degrees from Technische Universität Darmstadt, Darmstadt, Germany, in 2014 and 2017, respectively, where he is currently pursuing the Ph.D. degree with the Microwave Engineering Group. His current research interests include tunable microwave filters and material characterization.

HENNING TESMER was born in Kassel, Germany, in 1992. He received the B.Sc. and M.Sc. degrees from Technische Universität Darmstadt, Darmstadt, Germany, in 2015 and 2018, respectively, where he is currently pursuing the Ph.D. degree with the Institute of Microwave Engineering and Photonics. His current research interests include liquid crystal-based tunable dielectric waveguides and components for millimeter-wave applications.

JONATHAN STROBL was born in Dieburg, Germany, in 1996. He is currently pursuing the B.Sc. degree in electrical engineering and computer science. Since 2017, he has been a Student Assistant with the Institute for Microwave Engineering and Photonics, Technische Universität Darmstadt, where he has been developing automated high-voltage control systems for tunable microwave devices. His current research interests include microprocessor design and analog circuit engineering.

CHRISTIAN SCHUSTER (S'16) was born in Wiesbaden, Germany, in 1988. He received the B.Sc. and M.Sc. degrees from Technische Universität Darmstadt, Darmstadt, Germany, in 2012 and 2015, respectively, where he is currently pursuing the Ph.D. degree with the Microwave Engineering Group. His current research interests include tunable microwave filters and reconfigurable RF transceiver systems.

MATTHIAS NICKEL was born in Wetzlar, Germany, in 1987. He received the master's degree from the Technische Universität Darmstadt, in 2014, where he is currently with the Institute for Microwave Engineering and Photonics. His current research interests include active phased array antennas and liquid crystal-based microwave components for millimeter wave systems.

ANGEL BLANCO GRANJA was born in Palencia, Spain, in 1992. He received the B.Sc. degree in telecommunication technologies engineering from the University of Valladolid (UVa), in 2014, and the M.Sc. degree in telecommunications engineering from the Technical University of Denmark (DTU), in 2016. He is currently pursuing the Ph.D. with the Institut für Mikrowellentechnik und Photonik, Technische Universität Darmstadt (TuDa), in collaboration with the Technische Hochschule Mittelhessen (THM). He joined the Institut für Mikrowellentechnik und Photonik, TuDa, in 2016. His current research interest includes developing a new generation of Schottky diode-based envelope detectors at mm-waves and sub-terahertz frequencies.

ROLF JAKOBY (M'97) was born in Kinheim, Germany, in 1958. He received the Dipl.-Ing. and Dr.-Ing. degrees in electrical engineering from the University of Siegen, Germany, in 1985 and 1990, respectively.

In 1991, he joined the Research Center of Deutsche Telekom, Darmstadt, Germany. Since 1997, he has been a Full Professor with Technische Universität Darmstadt, Germany. He is currently a Co-Founder of ALCAN Systems GmbH. He has authored over 320 publications and holds more than 20 patents. His current research interests include chipless RFID sensor tags, biomedical sensors and applicators, and tunable passive microwave/millimeter wave devices and beam-steering antennas, using primarily ferroelectric and liquid crystal technologies.

Dr. Jakoby is a member of VDE/ITG and IEEE/MTT/AP societies. He received the Award from CCI Siegen for his excellent Ph.D. thesis, in 1992, and the ITG-Prize for an excellent publication in the IEEE TRANSACTIONS ON ANTENNAS AND PROPAGATION, in 1997. His group received 21 awards and prizes for best papers and doctoral dissertations. He was the Chairman of the EuMC, in 2007, and GeMiC, in 2011, and a Treasurer of the EuMW, in 2013 and 2017. He is the Editor-in-Chief of *FREQUENZ*(DeGruyter).

HOLGER MAUNE (S'07–M'12–SM'18) was born in Cologne, Germany, in 1981. He received the Dipl.-Ing. and Dr.-Ing. degrees in communications engineering from the Technische Universität Darmstadt, Darmstadt, Germany, in 2006 and 2011, respectively. His research focuses on reconfigurable smart radio frequency (RF) systems based on electronically tunable microwave components, such as phase shifters, adaptive matching networks, tunable filters, duplexer, and multiband antennas. Their integration into system components, such as adaptively matched power amplifiers, reconfigurable RF frontends, or fully integrated electronically beam-steering transceiver antenna arrays, is in the focus of the work.